

The Thermal Pressure of the Hot Interstellar Medium derived from Cloud Shadows in the Extreme Ultraviolet

Thomas W. Berghöfer

Space Sciences Laboratory, University of California, Berkeley, CA 94720, USA

Stuart Bowyer

Space Sciences Laboratory, University of California, Berkeley, CA 94720, USA

Richard Lieu

Department of Physics, University of Alabama, Huntsville AL 35899, USA

Jens Knude

Niels Bohr Institute for Astronomy, Physics, and Geophysics, University Observatory, Juliane Mariesvej 30, DK-2100 Copenhagen OE, Denmark

ABSTRACT

We have used the Deep Survey telescope of EUVE to investigate shadows in the diffuse EUV/Soft X-Ray background cast by clouds in the interstellar medium. We confirm the existence of a shadow previously reported, and provide evidence for two new shadows. We used IRAS data to identify the clouds producing these shadows and to determine their optical depth to EUV radiation. The EUV-absorbing clouds are optically thick in the EUV, and all EUV emission detected in the direction of these shadows must be produced from material in front of the clouds. We obtained new optical data to determine the distance to these clouds. We use a new differential cloud technique to obtain the pressure of the interstellar medium. These results do not depend on any zero level calibration of the data. Our results provide evidence that the pressure of the hot interstellar gas is the same in three different directions in the local interstellar medium, and is at least 8 times higher than derived for the local cloud surrounding our Sun. This provides new evidence for large thermal pressure imbalances in the local ISM, and directly contradicts the basic assumption of thermal pressure equilibrium used in almost all present models of the interstellar medium.

Subject headings: ISM: bubbles, clouds, general, structure — X-rays: ISM

1. Introduction

The discovery of the soft X-ray / EUV background (Bowyer, Field, & Mack 1968) and its anti-correlation with the Galactic HI distribution has led to an ongoing debate on the origin of that emission. Since an absorption column density of $N_{\text{HI}} = 1.2 \times 10^{20} \text{ cm}^{-2}$ (which corresponds to an optical depth $\tau = 1$ at 0.25 keV) is reached at a distance of approximately 100 pc in the direction of the Galactic plane, the diffuse background must arise from hot gas in the local interstellar medium (ISM). Optical and UV absorption line measurements of nearby stars together with observations in the X-ray and EUV wavelength range have established a local region with a significant HI deficiency which is partly filled with a plasma, the so-called “Local Bubble” (LB). No definite model exists for this region and its origin is unclear.

One view is that the gas in the LB has been heated by a supernova explosion which occurred in the solar neighborhood about 10^7 yr ago (cf. McKee & Ostriker 1977, Cox & Reynolds 1987). Other authors claim that the LB is part of an asymmetrically shaped superbubble created by stellar winds and supernova explosions (cf. Frisch 1995). However, the physical properties such as density, temperature, pressure, and extension of the LB, are not well determined and so far observational constraints are insufficient to establish a canonical model of the evolution and the origin of the LB. The McKee & Ostriker model is the best known model but it is not easily testable. Only soft X-ray and EUV observations provide a direct method to study the hot gas in the ISM and test LB models.

This paper presents new measurements for the thermal pressure in the local ISM, using observations of nearby clouds taken by the Deep Survey (DS) telescope on-board the *Extreme Ultraviolet Explorer* (EUVE). Prior to this paper, Bowyer et al. (1995) reported on the first detection of a spatial absorption feature in the diffuse EUV background; this feature was positionally coincident with an IRAS cirrus cloud at a distance of $\lesssim 40$ pc. Since the cloud casting this shadow is optically thick at EUV wavelengths, the authors concluded that all residual EUV emission observed at the position of the cloud originated from material along the line of sight in front of the cloud. By attributing the background subtracted flux in front of the cloud to the hot gas in the ISM, Bowyer et al. (1995) derived for the length of the emitting region (40 pc) a pressure (P/k) of $19,000 \text{ cm}^{-3}\text{K}$.

These authors pointed out that an imperfect zero level calibration of the data can lead to a smaller value for the pressure, and estimated a lower limit for the pressure of $7,000 \text{ cm}^{-3}\text{K}$.

The purpose of this paper is to present a re-observation of the previously reported cloud shadow in the EUV background and observations of two new shadows discovered in the DS. For all three shadow regions we provide new optical photometry data which establishes the distance of the respective clouds. We employ a differential cloud technique which does not depend on any zero level calibration, to obtain the pressure of the ISM in these directions.

The outline of this paper is as follows: First, in Sect. 2 we describe our new observations and the data analysis. In Sect. 3, we employ a new analysis technique and compare our results for the three cloud shadows. We derive physical quantities of the hot interstellar gas from our observations. Finally, in Sect. 4, we discuss the implications for models of the local ISM.

2. Observations and reduction methods

2.1. EUVE observations

After launch in June 1992 the EUVE satellite performed an all-sky survey in four bandpasses in the spectral range between 70 and 800 Å. Details about the EUVE mission and the instrumentation can be found in Bowyer & Malina (1991). Here we only summarize the capabilities of the DS instrument which has been used to obtain the EUVE data discussed in this paper. The DS instrument, consisting of a grazing incidence telescope and two broad band filters (Lexan/Boron filter: 65–190 Å, Al/Carbon filter: 160–385 Å) in front of an imaging microchannel plate detector, is mounted perpendicular to the other scanner telescopes. During the EUVE survey phase, the DS made deep exposures of the sky along the ecliptic plane. A schematic layout of the DS detector field can be found in Lieu et al. (1993). Owing to its anti-solar pointing direction, the DS instrument observed about $2^\circ \times 1^\circ$ of the Galactic plane per day. With a typical exposure of 20 ksec/pixel the DS is about a factor of 10 more sensitive than the EUVE all-sky survey. Generally speaking, diffuse emission is difficult to detect with microchannel plate detectors which exhibit a large instrumental background. It is thus clear that the DS data are better suited for a search for diffuse structures in the EUV background than the much

shorter exposed EUVE all-sky survey data.

Lieu et al. (1993) showed that the diffuse astrophysical background contributes about 25% of the total count rate observed in the Lex/B filter of the DS instrument, and used a ‘filter frame subtraction’ method to remove particle background contamination from the diffuse background data. The resulting Lex/B count rates were correlated with such terrestrial coordinates as satellite position, solar zenith angle and magnetic L-value, to identify and eliminate periods of data when the count rates are higher than the stable minimum value.

We first discuss our re-observation of lb165-32. As a naming convention for the shadowing clouds discussed here we use the letters “lb” followed by the Galactic coordinates of the cloud in degrees. In this re-observation we used a different observational technique than that employed in the original observation. The longitudinal side of the filter was maintained at a 90° orientation with respect to the ecliptic plane to maximize the exposed region above and below the plane. In the original observation during the EUVE DS this filter was constantly rotating about the DS axis. In both the original DS scan as well as in the re-observation, the same field of view of $1.53^\circ \times 0.49^\circ$, excluding the area of a dead spot ($0.093^\circ \times 0.069^\circ$) was observed. However, the rotating filter configuration during the DS leads to a shorter exposure of those parts of the scan located outside the inner 0.5° swath centered on the ecliptic plane. Depending on the size, shape, and orientation of the interstellar absorption feature, this could result in a difference between the DS and re-observation count rates. We carried out a series of tests with a variety of synthetic absorption features folded with the spatial detector response and established a change in the count rates by up to 20%.

In Figure 1 we plot a pulse height spectrum of the Lex/B filter counts detected during the re-observation of the cloud lb165-32. The observed spectrum presented in Figure 1 consists of a prominent Gaussian profile and an exponential background distribution. The Gaussian profile is typical of photon data from point sources and indicates that more than 90% of the diffuse counts are contributed by photons. This confirms and strengthens the results of Lieu et al. (1993) who showed using different techniques that we are detecting photons, not charged particles, in these observations. Our new analysis technique (discussed later), shows that about 50% of these photons are astronomical in origin. The nonastronomical photons are be-

lieved to be a combination of scattered geocoronal and solar EUV and X-ray emission.

In the upper panel of Figure 2, we plot our new results on the diffuse background as a function of the ecliptic longitude for lb165-32. For comparison, the original observation is shown in the middle panel; the plotted scan of the ecliptic plane begins at Galactic coordinates $l \approx 163.3^\circ, b \approx -34.3^\circ$ and ends at $l \approx 167.5^\circ, b \approx -29.5^\circ$. It is evident that an absorption feature is present in both data sets. The dashed lines (upper and middle panel) give the average background levels for the two scans outside the shadow region. In the case of the DS observation, this background has been determined from the scan range between ecliptic longitude 39° and 60° . For the re-observation we determined the background from the scan at ecliptic longitude above 52.5° and below 50.3° . The respective average diffuse background count rates are 0.495 ± 0.06 cts/s for the DS scan and 0.612 ± 0.026 cts/s for the re-observation; the count rates correspond to a field of view of 0.7433 square degree. In the lower panel of Figure 2 we plot an IR-emission scan across lb165-32 which we constructed from the continuum subtracted IRAS $100 \mu\text{m}$ sky map that has been folded with the spatial response of the rotating DS Lex/B filter region used to extract the EUV background scan across lb165-32. As can be seen from Figure 2, the absorption feature in the EUVE data is positionally coincident with an enhanced emission feature in the IRAS $100 \mu\text{m}$ data in the ecliptic plane near ecliptic longitude $l = 52^\circ$. In both independent EUVE observations the absorption feature appears with a significance of $3 - 3.5 \sigma$ below the average background level. These two independent measurements, both at greater than 3σ leave no doubt about the detection of this shadow in the EUV background.

Modeling of synthetic absorption profiles folded with the detector spatial responses shows that the different shape of the absorption feature and the roughly 20% higher count rates during the re-observation of lb165-32 is explained by the modified observing technique used in the re-observation.

For the DS scan of lb165-32 we find at the position of the cloud a minimum count rate of 0.35 ± 0.06 cts/s. From the scan regions immediately adjacent to the cloud ($l = 50.0 - 50.6^\circ$ and $l = 53.3 - 54.8^\circ$) we determine a local continuum diffuse EUV background rate of 0.51 ± 0.06 cts/s.

We have found a second absorption feature in the EUV background which we designate as lb27-

31. In the upper panel of Figure 3 we show the EUVE DS scan of the ecliptic plane near ecliptic longitude $l = 309.5^\circ$ beginning at Galactic coordinates $l \approx 24.9^\circ, b \approx -29.0^\circ$ and ending at $l \approx 32.0^\circ, b \approx -37.0^\circ$. The lower panel of Figure 3 shows the IR emission for this sky location. Both the EUV background as well as the IR emission have been reduced in the same way as described for lb165-32. The EUV background absorption feature in the Galactic plane centered near ecliptic longitude $l = 309.0^\circ$ appears at the position of an IRAS cirrus cloud. Again, a comparison of the EUVE DS data with the IRAS $100\mu\text{m}$ data provides evidence for a prominent (5σ) shadow in the EUV background cast by a cloud in the local ISM. The minimum count rate of 0.48 ± 0.03 cts/s at the position of the shadowing cloud is taken from the data point at $l = 309^\circ$. By averaging the observed count rates between $l = 305 - 307^\circ$ and $l = 311 - 313^\circ$, we determine a local continuum count rate of 0.61 ± 0.03 cts/s,

A third cloud shadow (designated as lb329+46) was found in the DS data in the range $l = 209 - 216^\circ$ (corresponding to Galactic coordinates between $l \approx 324.4^\circ, b \approx 49.4^\circ$ and $l \approx 332.0^\circ, b \approx 44.6^\circ$). This scan is shown in Figure 4. With respect to the mean DS Lex/B diffuse background count rate (dashed line in Figure 4), taken from the scan range between $l = 205 - 220^\circ$ excluding the region $l = 210 - 215^\circ$, the EUV background exhibits a 4σ absorption feature between $l = 212.5 - 215^\circ$ as well as an enhanced emission feature near $l = 211^\circ$. The comparison with the IRAS $100\mu\text{m}$ data shows that the absorption feature is spatially coincident with two IR emission features near $l = 212.8^\circ$ and $l = 214^\circ$; the IRAS $100\mu\text{m}$ sky map shows two finger-like emission structures crossing the ecliptic plane at these positions (note that the zero flux of the IR scan is a result of the subtracted continuum which has been taken from the region near $l = 211^\circ$). We adopted a count rate of 0.36 ± 0.05 cts/s for the position of the shadow. From the regions near $l = 212^\circ$ and $l = 215.5^\circ$ we obtain a local EUV background count rate of 0.57 ± 0.05 cts/s.

The significantly lower IR emission near $l = 211^\circ$ indicates a much lower absorption column in this direction. The higher EUV emission (0.70 ± 0.05 cts/s) in this region can be explained by a larger emission column along this line of sight.

2.2. Optical observations

In this subsection we present our optical observations of stars in the direction of these shadows. In order to determine the distance to the EUV-absorbing clouds we have used detailed Strömgren photometry; this technique has been shown to provide the absolute magnitude and reddening of most classes of main-sequence stars (cf. Strömgren 1966, Crawford 1979, Olsen 1988). All photometry was carried out with the Strömgren automatic telescope at ESO La Silla, Chile. The stars for observation were selected from the position and proper motion star catalog (Röser & Bastien 1991) and the Space Telescope guide star catalogue (Lasker et al. 1990). The error propagation of the $uvby\beta$ indices result in a typical error of roughly 15% for the distance to the stars investigated. For 34 of our 210 program stars Hipparcos parallaxes exist. For these stars the distances obtained by Strömgren photometry agree within the errors of the Hipparcos measurements. This provides confirmation of the accuracy of our distance estimates for the overlapping stars. A detailed discussion of this comparison including all our optical data of the individual stars in the cloud regions can be found in Knude (1997). In Table 1 we provide a summary of the optical data of the stars that we use to establish the distance of the shadowing clouds. For each of these 8 stars, Table 1 provides the position in Galactic coordinates, the distance derived from our photometry data and from the Hipparcos data, and the reddening E_{b-y} .

For each cloud region we show a plot of the color excesses versus distance (Figure 5, 7, and 9) as well as a plot of the location of the stars (Figure 6, 8, and 10) in relation to the cloud shadows. We use different symbols to discriminate between reddened stars (filled symbols) and almost unreddened stars (open symbols). A threshold of $E_{b-y} = 0.02$ has been chosen which is related to an optical depth exceeding unity in the DS Lex/B filter band. According to the relation $N_{\text{HI}}(\text{atoms}/\text{cm}^2) = (7.5 \pm 1.0) \times 10^{21} E_{b-y} - (8.7 \pm 0.55) \times 10^{19}$ (Knude 1978), a value of $E_{b-y} = 0.02$ is equivalent to an interstellar HI absorption column density of $6.3 \times 10^{19} \text{atoms}/\text{cm}^2$. In principle, the distance of the EUV-shadowing clouds can be constrained by finding the most distant unreddened star in front of a cloud and the closest reddened star behind this cloud. This method can also be applied to determine the distance where optical depth reaches unity in the regions immediately adjacent to the shad-

Table 1: Summary of stellar data constraining the distance of the shadowing clouds

Name	gal. Coord. l, b	Distance (pc)		E_{b-y} mag
		phot.	Hipp.	
HD 20065	51.034, 0.298	39.0	40.8	0.029
HD 20477	51.975, -0.092	52.0	52.1	0.020
HD 197818	309.416, 0.761	43.0	35.1	0.017
HD 197212	307.980, -1.257	47.0		0.120
HD 198902	310.645, -1.486	53.0	66.8	0.076
HD 196617	307.839, 1.809	56.0	55.7	0.035
HD 123453	214.269, 0.015	47.0	62.3	0.018
HD 123829	214.890, -0.206	73.0		0.022

owing cloud which we need for our new differential cloud technique (see Sect. 3.1).

In Figure 5 we show a plot of the color excesses E_{b-y} versus stellar distances for all of our program stars in the region of lb165-32. Figure 6 shows the positions of our program stars and the location of the EUV-absorbing / IR-emitting cloud in the scan path of the EUVE satellite along the ecliptic plane; two horizontal lines at $\pm 0.76^\circ$ indicate the width of the field of view of the DS instrument that has been used to obtain the EUV background. Of the ~ 150 stars observed in the lb165-32 region, 57 met the criteria required to establish distances using the uvby β system. As can be seen from Figure 5, 4 stars at distances less than 100 pc (filled squares in Figure 5) show reddening larger than $E_{b-y} > 0.02$. Together with the IRAS $100 \mu\text{m}$ sky map, the data in Figure 6 confirm that the reddening is caused by the cirrus cloud in the ISM that is also responsible for the EUV-absorption; the shaded area in Figure 6 represents the FWHM area defined by the width of the IR-emission / EUV-absorption feature (cf. Figure 2) in the direction of the ecliptic plane and the FWHM of the detector response in ecliptic latitude direction. Since all unreddened stars appear outside the cloud boundary and are also located at distances $D > 40$ pc, the closest reddened star places a limit to the distance of the cloud of $D \lesssim 40$ pc. Most stars located beyond 100 pc (triangles in Figure 5), show reddening values well above $E_{b-y} > 0.05$. The location of these stars indicate a second much larger cloud behind the nearby EUV-absorbing cloud. This larger, more distant cloud limits the emitting length for a local continuum in the diffuse EUV background emission in this direction. The EUV emission must originate in

front of 100 pc.

Figure 6 shows three stars of low reddening and distances beyond 100 pc (open triangles) inside the cloud boundary (shaded area). At the position of these stars the IRAS $100 \mu\text{m}$ sky map shows a locally lower emission level, thus indicating inhomogeneity in the shadowing cloud. Compared to the entire shadow areas these smaller “holes” cover less than $\approx 10\%$ and their influence on the EUV background scan is low.

In Figure 7 we have plotted E_{b-y} against distance for stars in the sky region around lb27-31. Figure 8 provides the positions of the stars in relation to the cloud shadow; the labeling of the data points is the same as used in Figure 5 and Figure 6. A number of the nearby stars ($D < 100$ pc) show significant extinction up to $E_{b-y} = 0.12$ mag. Two of these stars are located within the shaded area of Figure 8 (which marks the most prominent position of the cloud shadow in the EUVE scan). Together with the closest star ($D = 42$ pc) in our sample which shows an extinction somewhat below the threshold of $E_{b-y} = 0.02$, the highly reddened nearby stars indicate a distance of $D \approx 45$ pc for the shadowing cloud. We note that the almost unreddened star at $D = 42$ pc is located at ($l = 309.2^\circ, b = -0.7^\circ$), right below the shaded area in Figure 8. At $D \approx 130 - 140$ pc there is a boundary, beyond this boundary a large number of stars have significant extinctions with $E_{b-y} \geq 0.05$ mag. This indicates a second cloud behind the cloud at $D \approx 45$ pc. The distribution of the reddened stars at larger distances (filled triangles in Figure 8) confirms the larger extent of this second cloud. We use a distance of 135 pc to establish the emitting length of the EUV background continuum to this second cloud

The optical data for the third interstellar absorp-

tion feature casting a shadow in the diffuse EUV background emission (lb329+46) are shown in Figures 9 and 10. Again, the E_{b-y} versus distance plot indicate the existence of two clouds positioned at distance of $D \approx 65$ pc and $D \lesssim 125$ pc. The positions of the reddened stars at $D = 62$ pc ($l = 214.269^\circ, b = 0.015^\circ$) and $D = 73$ pc ($l = 214.890^\circ, b = -0.206^\circ$) are coincident with the most prominent absorption feature in the EUV background scan (cf. Figure 4). The somewhat more distant but unreddened stars in the EUVE scan region between $l = 213.4 - 214.2^\circ$ indicate less absorbing material in this sky direction which is consistent with the higher Lex/B count rate in this range. From the E_{b-y} and distance values of the stars located near ecliptic longitude $l = 211^\circ$ we determine an upper limit of $D \approx 180$ pc for the distance where optical depths reaches unity (in the EUV).

In all three cloud shadows reported here, our optical data provide evidence for a second larger cloud located behind the nearby EUV-absorbing cloud. In order to prevent any confusion regarding the different clouds and the different lines of sight we use the following convention: the nearby cloud casting the shadow in the EUV background is designated as the “shadowing cloud”. The second more distant cloud is denoted as the “background cloud”.

3. Analysis

3.1. The differential cloud technique

We developed a new method to measure the EUV background flux by means of EUVE DS observations of nearby clouds in the local ISM, which is independent of any zero level calibration of the detector. In order to set up this new differential cloud technique the EUVE scan across a cloud must cover the shadowing cloud as well as enough regions adjacent to the shadowing cloud for a local continuum flux determination in front of the background cloud. We note that this method only works when a smaller cloud is located in front of a larger, more distant cloud as in the case presented here for our three cloud shadows. Since the EUVE fluxes obtained in the direction of the nearby clouds and the more distant background clouds are contaminated by the same amount of nonastronomical background, the comparison of the flux at the position of the shadowing cloud with the continuum flux originating in front of the background cloud provides a differential measurement of the EUV background.

Figure 11 schematically shows our new differential cloud technique. The observed flux deficit Δ at the position of the shadowing cloud (with respect to the local continuum emission in front of the background cloud) is associated with a specific emitting length L along the line of sight, namely the distance between the front of the shadowing cloud and the background cloud.

3.2. Cloud shadow results

In Table 2 we provide a summary of the results for our three cloud shadows. For each cloud, both the shadowing clouds and the background clouds, we give its distance and the corresponding DS Lex/B filter count rate. For lb165-32 we use the count rates obtained during the original observation, so that all the count rates are from the same observation mode (i.e. the DS). A third measurement given for lb329+46 is from a location near lb329+46 showing a significantly higher EUV flux (cf. Sect. 2.1 and Sect. 2.2) and a significantly larger free path.

In Figure 12 we plot the DS Lex/B filter count rates versus the respective distances for all three cloud shadows. The different cloud shadow regions are marked by different symbols, the distance upper limits are indicated by left arrows. As is evident from Figure 12 almost all the data points are reasonably fit with a straight line. We performed several correlation tests and confirmed the existence of a tight correlation between the DS Lex/B filter count rates and the distances of the clouds. The formal results of a parametric linear regression analysis of the data (including the two distance upper limits) are 0.002 ± 0.0003 cts/s pc $^{-1}$ for the slope and 0.331 ± 0.045 cts/s for the intercept of the regression line. This line is plotted in Figure 12. The slope of the regression line gives the diffuse EUV flux per emitting length which we use to derive the pressure of the plasma in the ISM. Figure 12 includes the regression lines (dotted lines) for the individual lines of sight. The individual lines of sight show slopes between 0.0015 cts/s pc $^{-1}$ (lb27-31) and 0.0027 cts/s pc $^{-1}$ (lb165-32) which deviate by -25% and +35% from the value obtained by the regression analysis including all clouds. We believe these limits reflect all uncertainties due to possible variations of the absorption column in the foreground of the different clouds, and within these uncertainties all data of all three lines of sight can be explained by the same slope. In the next section, where we compute the pressure of the hot ISM gas, we show that these

Table 2: The observed DS Lex/B count rates and the distances for the respective clouds.

cloud	Distance (pc)	Lex/B cts/s
lb165-32	$\lesssim 40$	0.35 ± 0.06
	100 ± 20	0.51 ± 0.06
lb27-31	45 ± 10	0.48 ± 0.03
	135 ± 20	0.61 ± 0.03
lb329+46	65 ± 10	0.36 ± 0.05
	125 ± 20	0.57 ± 0.05
	$\lesssim 180$	0.7 ± 0.05

uncertainties can affect the inferred pressure value by only 10–15%. The tight correlation between observed diffuse EUV flux and emitting length implies essentially the same pressure in all three cloud directions. In Figure 13 we show a plot of the cloud locations in a projection from above the Galactic plane. As can be seen the detected EUV-absorbing clouds are located in three significantly different directions. This is important for our conclusions for the hot gas in the ISM and is further addressed in Sect. 4.

An additional point is that the y-intercept provides a zero level calibration for our cloud shadow observations with the EUVE DS instrument. This zero level can be used to subtract the nonastronomical photons from the EUVE observations and allows us to measure absolute fluxes for the diffuse EUV background; we note that about 50% of all detected photons are astronomical in origin. Consequently, the pressure value derived from the slope of the regression line not only provides the average pressure of the material in the distance range $\approx 40 - 180$ pc (between the shadowing cloud and the larger background cloud), it also allows us to determine the thermal pressure of the ISM in the regions in front of the three clouds. It is noteworthy that these zero level corrected values also give the same pressure for the material in the foreground of the three shadowing clouds. We point out that intrinsic absorption along the lines of sight can have flattened the apparent correlation between EUV flux and distance. Therefore, the given value for the y-intercept represents an upper limit.

3.3. The pressure of the ISM

We now utilize the results of our cloud shadow observations to compute the pressure of the local ISM

from the ideal gas law

$$P/k = 1.92 \cdot \sqrt{\text{EM/L}} \cdot T \quad (1)$$

where P is the pressure, k is the Boltzmann's constant, EM/L is the emission measure per emitting length, and T is the temperature; the factor of 1.92 accounts for the number of free particles (electrons + ions) in the plasma. The conversion of the observed EUVE DS count rates per emitting length into EM/L is model dependent. A detailed discussion of the implications of different plasma models and plasma emissivity codes on the pressure of the local ISM will be given elsewhere. Here we use the typically assumed model spectrum of a plasma in collisional ionization equilibrium at a temperature of 10^6 K. To account for absorption in the foreground of the clouds we include a foreground ISM absorption column of $N_{\text{H}} = 5 \times 10^{18} \text{ cm}^{-2}$ in our model. With the plasma emissivity code provided by Landini & Monsignori-Fossi (1990) we derive $\text{EM/L} = 7.3 \times 10^{-5} \text{ cm}^{-6}$ and a pressure $P/k \approx 16500 \text{ cm}^{-3} \text{ K}$; for a Raymond & Smith (1977) model of the same parameters we obtain $\text{EM/L} = 5.1 \times 10^{-5} \text{ cm}^{-6}$ and $P/k \approx 13500 \text{ cm}^{-3} \text{ K}$. The column density of the local cloud around our Sun in the three view directions varies between $N_{\text{H}} = 5 \times 10^{17} \text{ cm}^{-2}$ (lb27-31) and $N_{\text{H}} = 3 \times 10^{18} \text{ cm}^{-2}$ (lb165-32) (P. Jelinsky 1998, private communication). This might explain some of the deviation between the data obtained in the individual view directions. However, a 10 times lower absorption column density affects the inferred emission measure by 30% and thus results in an uncertainty of the pressure value of only 15%. Any significant absorption by cold gas in front of the clouds exceeding $N_{\text{H}} = 5 \times 10^{18} \text{ cm}^{-2}$ would depress the apparent diffuse EUV flux with increasing emitting length in the ISM and, thus, increase the pressure of the hot gas in

the ISM.

We point out that the variation in the pressure value resulting from the use of different plasma emissivity codes (which is a general problem in high energy astrophysics) exceeds the error in the determination of the EUVE DS count rate per emitting length as derived from the slope of the regression line in Figure 12. The latter results in an error of 10–15% for the pressure value. Strictly speaking, our value represents a lower limit for the actual value of the pressure. Because we measure the count rate deficit at the position of a shadowing cloud against the local background, any flux contribution from behind the shadowing clouds reduces the respective count rate deficit. Since we cannot definitely exclude such contributions, the actual value for the slope of the regression line can be higher. Additional intrinsic absorption along the lines of sight strengthens this effect. Therefore, the derived value $P/k = 16500\text{cm}^{-3}\text{K}$ provides a lower limit for the pressure of the local ISM.

4. Summary and Conclusions

We have presented a re-observation of a cloud shadow in the diffuse EUV background discovered by Bowyer et al. (1995) and present two additional shadows detected in the EUVE DS.

We have developed a new method to derive the diffuse astrophysical EUV background from the EUVE DS data. This differential cloud technique can be applied to any cloud shadow data without a known zero level calibration. In our case we can extrapolate the results to the origin and obtain a zero level calibration for the DS detector. This zero level calibration indicates that about 50% of the detected photons are astronomical in origin. More importantly, this zero level calibration allows a determination of the diffuse EUV background in the direction of the three nearby cloud shadows and hence to derive the pressure in the regions between us and these clouds. The pressure obtained for these nearby regions is consistent with the value obtained from the differential measurements for the more distant regions along the lines of sight.

The results of our cloud shadow observations with EUVE provide evidence for a constant pressure in three different directions in the local ISM. We derived a pressure of $P/k \approx 16500\text{cm}^{-3}\text{K}$. The canonical value obtained from the analysis of solar He I 584\AA radiation resonantly scattered by helium in the inflowing cloud is $P/k = 730 \pm 30\text{cm}^{-3}\text{K}$ (e.g.,

Frisch 1995). Based on line measurements with EUVE, Vallerga (1996) derived a pressure for the solar cloud in the range $P/k = 1700 - 2300\text{cm}^{-3}\text{K}$ which is in good agreement with results obtained by Bertaux et al. (1985), $P/k \approx 2600\text{cm}^{-3}\text{K}$. A comparison of these results shows the pressure of the local ISM exceeds the pressure of the cloud surrounding our Sun by a factor of ≥ 8 . The original observation (Bowyer et al. 1995) of a pressure imbalance between the solar cloud and the surrounding local ISM could have been the result of a nearby shock wave which had not yet reached the Sun. The results reported here are obtained in three different directions. The isotropy in the results for all these directions is not consistent with this hypothesis.

Flux in the soft X-ray bandpass requires a larger absorption column density to reach unit optical depth and it is difficult or impossible to separate the locally produced diffuse soft X-ray emission from contributions originating at larger distances. Soft X-ray observations, therefore, typically provide only an upper limit for the pressure of the local ISM. As discussed previously, the pressure obtained from our cloud shadow observations in the EUV is strictly interpreted as a lower limit. Although different plasma codes have been used by different authors, the pressure derived from our cloud shadow observations with EUVE is about the same as values derived from soft X-ray observations (e.g., Snowden 1998, Freyberg 1998) when we use the same code ($P/k(\text{EUV}) = 13500\text{cm}^{-3}\text{K}$; $P/k(\text{soft X-ray}) = 14000\text{cm}^{-3}\text{K}$). The near equality of these upper and lower limits implies we have measured the true pressure.

Beyond the cloud surrounding our Sun we found no significant intrinsic cold gas absorption in the local ISM. This supports the idea of a cavity primarily filled with an ionized plasma. Interstellar absorption lines in the spectra of nearby stars have indicated the existence of cloudlets of cold gas (like the local cloud around our Sun) in the solar vicinity (Lallement 1996). However, the effect of these cloudlets on the diffuse EUV emission observed in the directions of the cloud shadows discussed here is negligible. We point out that the different line of sights for the six clouds discussed here show that the local ISM cannot be simply described as a sphere with an almost constant radius (Snowden et al. 1990).

Our observations provide evidence for a large pressure imbalance in the local ISM compared to the local cloud surrounding our Sun. This contradicts the basic assumption of almost all available models for the lo-

cal ISM of a pressure equilibrium (e.g., McKee & Ostriker 1977, Cox & Reynolds 1987). It is unclear what physical mechanism can maintain such a large pressure imbalance. We emphasize that these models as well as the calculations in the here presented work assume a hot plasma in collisional ionization equilibrium. A completely different approach is provided by Breitschwerdt & Schmutzler (1994). Their model calculations are based on an adiabatically cooling non-equilibrium plasma. The advantage of this model is that it can at least qualitatively explain many of the observed features of the local ISM and it does not require pressure equilibrium in the local ISM.

We thank M. Lampton and J. Vallergera for useful discussions. T.W.B. acknowledges the support from the Alexander-von-Humboldt-Stiftung (AvH) by a Feodor-Lynen Fellowship. This work has been supported by NASA contract NAS 5-30180. R.L. is supported by NASA grant 5-34378 awarded to UAH. J.K. thanks the European Southern Observatory for observing time and travel support.

REFERENCES

- Bowyer, S., Field, G. B., Mack, J. E., 1968, *Nature*, 217, 32
- Bowyer, S., Malina, R. F. 1991, in *Extreme Ultraviolet Astronomy*, ed. R. F. Malina and S. Bowyer, (New York: Pergamon), 397
- Bowyer, S., Lieu, R., Sidher, S. D., Lampton, M., Knude, J. 1995, *Nature*, 375, 212
- Bertaux, J. L., Lallement, R., Kurt, V. G., Mironova, E. N., 1985, *A&A*, 150, 1
- Breitschwerdt, D., Schmutzler, T., 1994, *Nature*, 371, 774
- Cox, D. P., Reynolds, R. J., 1987, *ARA&A*, 25, 303
- Crawford, D. L., 1979, *AJ*, 84, 1858
- Freyberg, M. J., 1998, *Lecture Notes in Physics*, “The local bubble and beyond”, ed. D. Breitschwerdt, Springer-Verlag, in press
- Frisch P. C., 1995, *Space Sci. Rev.*, 72, 499
- Knude, J., 1978, in “*Astronomical papers dedicated to Bengt Strömberg*”, Copenhagen University Observatory, Copenhagen, p. 273
- Knude, J., 1997, *A&AS*, submitted
- Lallement, R., 1996, *Space Sci. Rev.*, 78, 361
- Landini, M., Monsignori-Fossi, B. C., 1990, *A&AS*, 82, 229
- Lasker, B. M., Sturch, C. R., McLean, B. J., et al., 1990, *AJ*, 99, 2019
- Lieu, R., Bowyer, S., Lampton, M., Jelinsky, P., Edelstein, J. 1993, *ApJ*, 417, L41
- McKee, C. F., Ostriker, J. P., 1977, *ApJ*, 218, 148
- Olsen, E. H., 1988, *A&A*, 189, 173
- Raymond, J. C., Smith, B. W., 1977, *ApJS*, 35, 419
- Röser, S., Bastien, U., *Position and Proper Motion Star Catalogue (Spektrum, Heidelberg)*, 1991
- Snowden, S., Cox, D. P., McCammon, D., Sanders, T., 1990, *ApJ*, 354, 211
- Snowden, S., 1998, *Lecture Notes in Physics*, “The local bubble and beyond”, ed. D. Breitschwerdt, Springer-Verlag, in press
- Strömberg, B., 1966, *ARA&A*, 4, 433
- Vallergera, J., 1996, *Space Sci. Rev.*, 78, 277

This 2-column preprint was prepared with the AAS L^AT_EX macros v4.0.

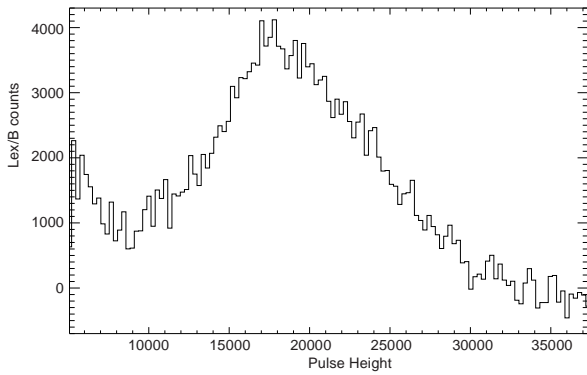


Fig. 1.— Pulse height spectrum of the Lex/B filter counts observed during the re-observation of lb165-32. The large roughly Gaussian peak is identical to that seen in observations of EUV point sources showing that most of the counts registered in this observation are due to photons.

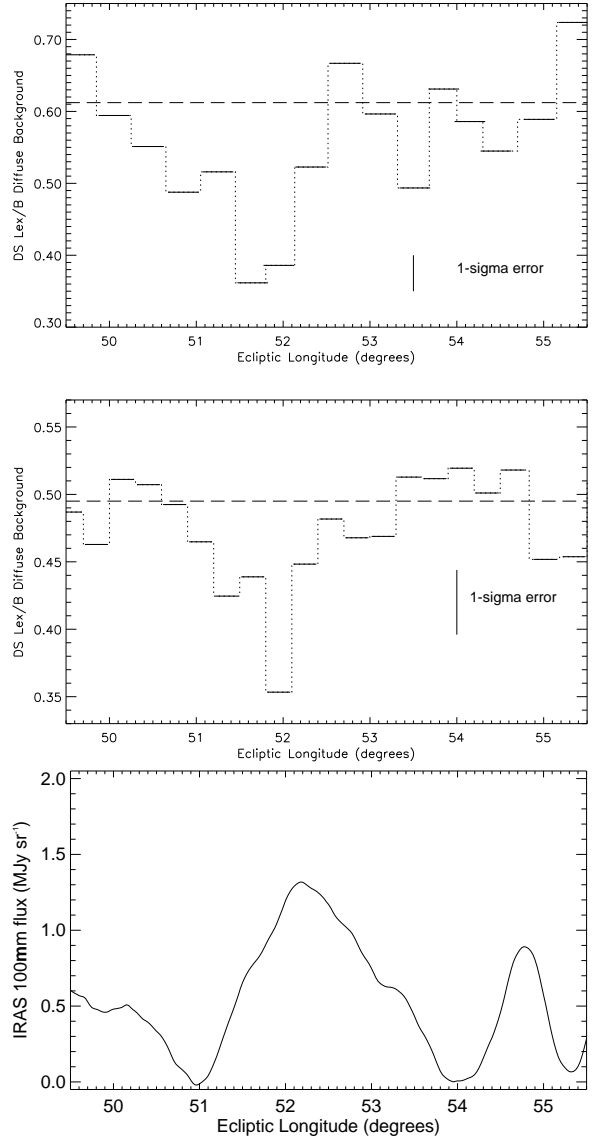


Fig. 2.— EUV diffuse background count rate in the Lex/B filter as a function of ecliptic longitude; the upper panel shows the new observation of lb165-32, the middle panel represents the same section obtained during the Deep Survey. The dashed lines correspond to the average background levels (cf. Sect. 2.1). For comparison, the lower panel shows the IR emission scan constructed from the continuum subtracted IRAS $100\mu\text{m}$ sky maps folded with the spatial response of the DS Lex/B filter.

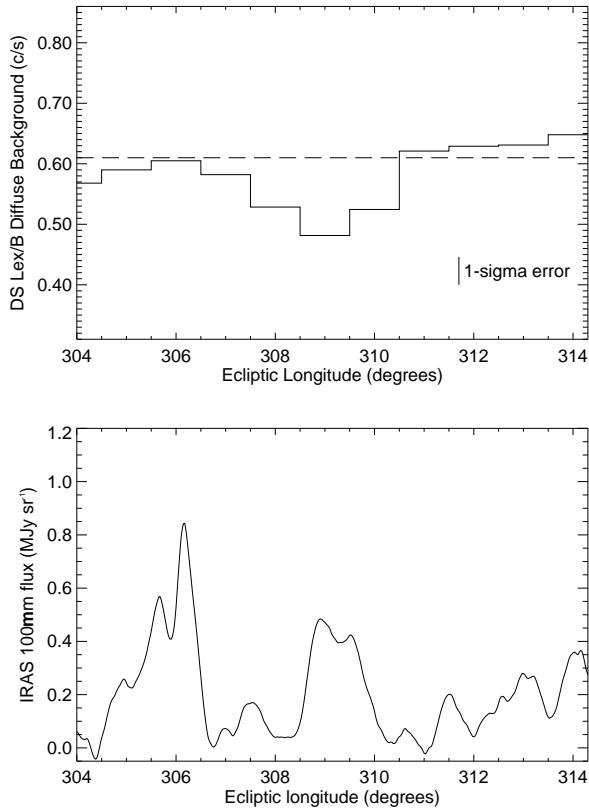


Fig. 3.— Plot of the EUV background scan across lb27-31 and the respective IR $100\mu\text{m}$ emission scan (cf. middle and lower panel of Figure 2).

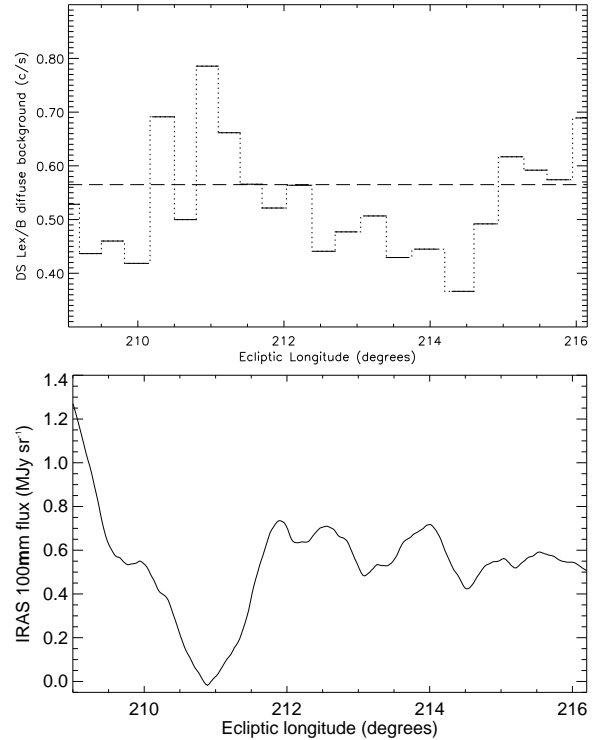


Fig. 4.— EUV diffuse background count rate in the Lex/B filter as a function of ecliptic longitude; the upper panel shows the new observation of lb329+46, the lower panel shows the IR emission scan constructed from the continuum subtracted IRAS $100\mu\text{m}$ sky maps folded with the spatial response of the DS Lex/B filter.

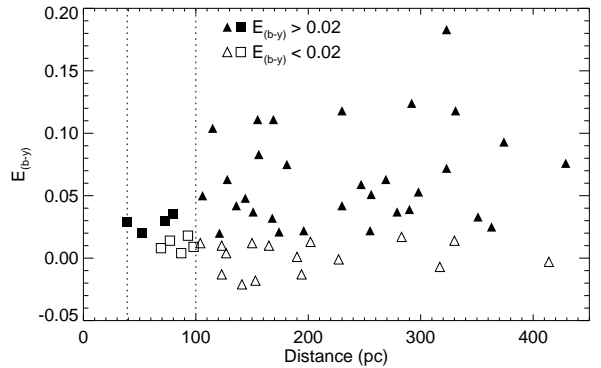


Fig. 5.— Color excesses E_{b-y} versus distances for stars near lb165-32; triangles and squares belong to distances $D > 100\text{ pc}$ and $D < 100\text{ pc}$, open and filled symbols represent excesses $E_{b-y} < 0.02\text{ mag}$ or $E_{b-y} > 0.02\text{ mag}$, respectively. Dotted lines indicate the distances of the two clouds (see Sect. 2.2).

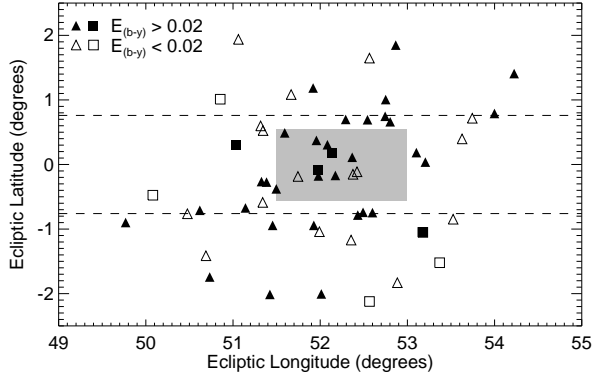


Fig. 6.— Location of stars shown in Figure 5; same symbols used as in Figure 5. The shaded area belongs to the FWHM of the IR-emission / EUV-absorption feature in Figure 2 and the FWHM of the EUVE scan perpendicular to the Galactic plane, the dashed lines show the sky area covered by the EUVE observations.

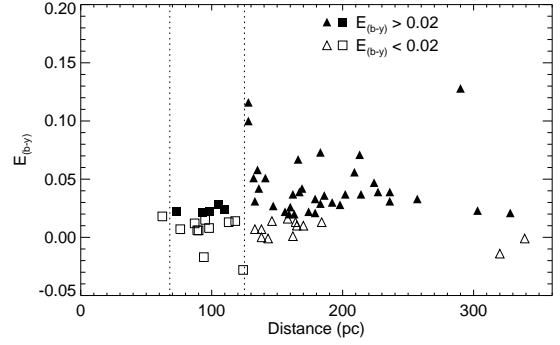


Fig. 9.— Same as Figure 5 for the shadow region lb329+46; the distance to the background cloud is 135 pc.

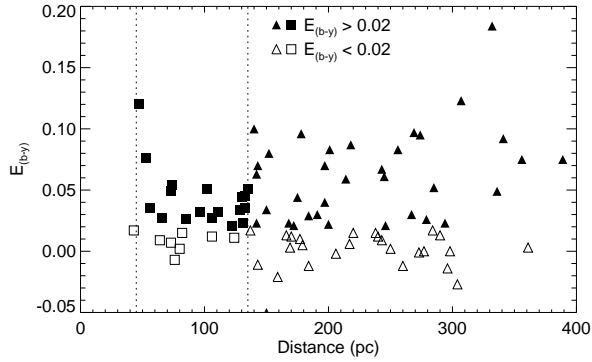


Fig. 7.— Same as Figure 5 for the shadow region lb27-31; the distance to the background cloud is 125 pc.

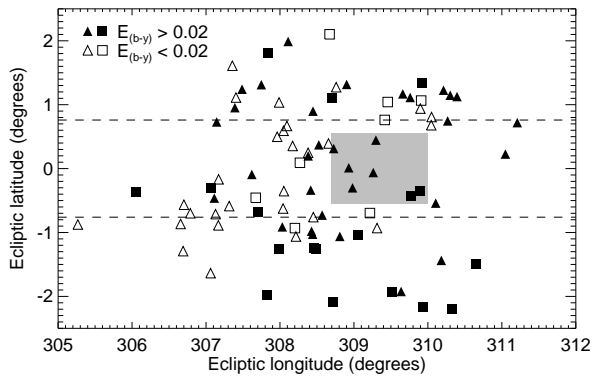


Fig. 8.— Same as Figure 6 for the shadow region lb27-31.

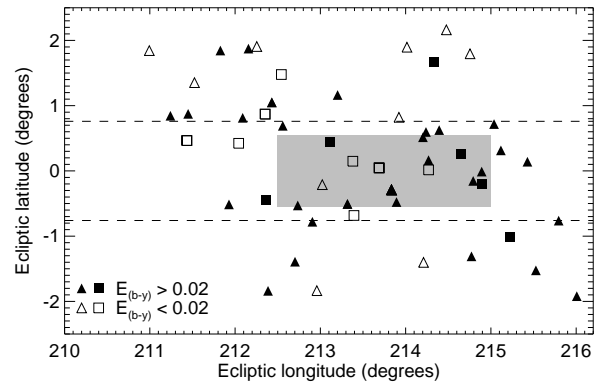


Fig. 10.— Same as Figure 6 for the shadow region lb329+46.

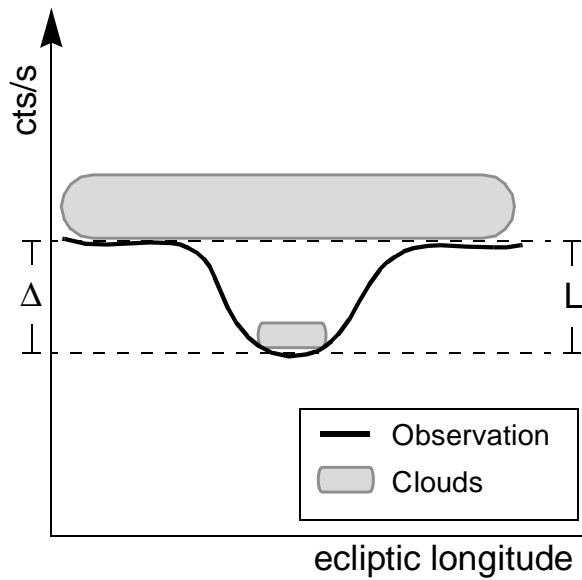


Fig. 11.— Sketch of our new differential cloud technique. A configuration of two clouds is overplotted with the EUV background scan (solid line) across the smaller nearby shadowing cloud. The local EUV background continuum behind the shadowing cloud originates in front of the second, larger and more distant background cloud. The observed count rate deficit Δ is associated with the column L between the two clouds in the ISM along the line of sight.

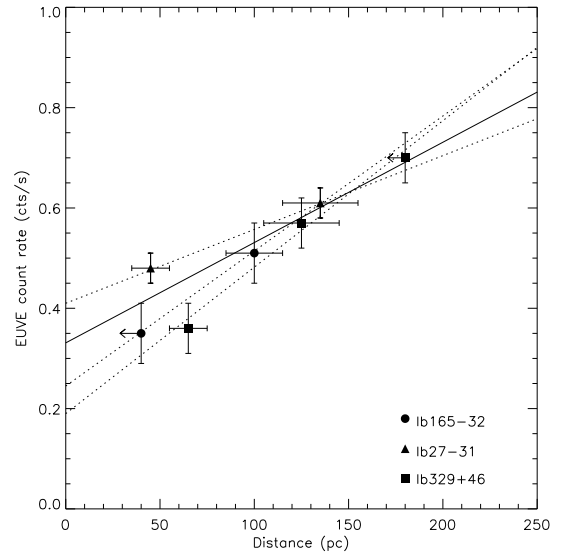


Fig. 12.— Plot of the observed count rates versus the distance of the respective clouds; distance upper limits are indicated by left arrows. The solid straight line provides the results of a parametric linear regression analysis (slope: 0.0020 ± 0.0003 cts/s pc $^{-1}$, intercept: 0.331 ± 0.045 cts/s, see text). The dotted lines show the individual results for the different lines of sight (see text).

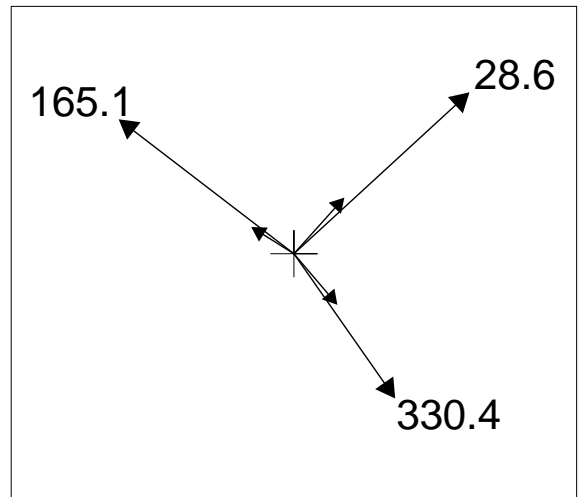


Fig. 13.— Projection of the sky directions towards the cloud shadows as seen from above the Galactic plane; numbers give the Galactic longitude, the length of the arrows scales with the projected distance of the clouds.